RSC Advances

PAPER

View Article Online
View Journal | View Issue

Cite this: *RSC Adv.*, 2016, **6**, 27452

Development of the catalytic reactivity of an oxo–peroxo Mo(VI) Schiff base complex supported on supermagnetic nanoparticles as a reusable green nanocatalyst for selective epoxidation of olefins†

Abolfazl Bezaatpour,*[a] Sahar Khatami[b] and Mandana Amiri[a]

Received 25th December 2015
Accepted 2nd March 2016

DOI: 10.1039/c5ra27751e

www.rsc.org/advances

A novel ancillary branch coated oxo–peroxo Mo(VI)tetradentate Schiff base complex on superparamagnetic nanoparticles was prepared and characterized by IR spectroscopy, X-ray powder diffraction (XRD), scanning electron microscopy (SEM), transmission electron microscopy (TEM), vibrating sample magnetometry (VSM), diffuse reflectance spectra (DRS) and atomic absorption spectroscopy (AAS). The catalyst was used for the selective epoxidation of cyclooctene, cyclohexene, styrene, indene, α-pinene, 1-hepten, 1-octene, 1-dodecen and *trans*-stilben using *tert*-butyl hydroperoxide as an oxidant in 1,2-dichloroethane. This catalyst is efficient for the oxidation of cyclooctene, with a moderate 100% selectivity for epoxidation with 97% conversion in 30 min. We were able to separate the supermagnetic nanocatalyst by using an external magnetic field, and to use the catalyst at least five successive times without significant decrease in conversion. The proposed supermagnetic nanocatalyst has advantages in catalytic activity, selectivity, catalytic reaction time and reusability by easy separation.

Introduction

Catalytic epoxidation of olefins is an interest of many researchers for the synthesis of fine chemicals. Because of their versatility as intermediates, epoxies are of great value in both synthetic organic chemistry and chemical technology.[1] Molybdenum(VI) Schiff base complexes have been intensively used as oxidation catalysts for a variety of organic substrates, because molybdenum complexes offer significant advantages such as being economic, environmentally friendly and commercially available.[2] Oxo–peroxo molybdenum complexes investigated particularly for epoxidation of olefins.[3–6] The catalytic activity of peroxido molybdenum complexes is related on the number of peroxido ligands attached to the catalyst and the nature of the remaining ligands in the coordination sphere.[7,8]

TBHP is environment-friendly and has good thermal stability.[9] Moreover, one of the main problems of homogeneous transition metal complexes as catalysts is the formation of oxo and peroxo dimeric and other polymeric species.[10] The formation of these compounds can deactivate catalysts irreversibly. This problem may be solved by immobilizing of the metal complexes within the solid supports so it can separate complexes from each other.[11] Meanwhile, the separation, recycling, insufficient stability of homogeneous catalysts and leaching of the active metal into the solvent are part of serious problems. Immobilization of the homogeneous metal complex onto solid supports has been the subject of a lot of research in catalytic fields because of long catalytic lifetime, easy separation, thermal stability, high selectivity and easy recyclability.[12–14] A main method for heterogenizing of homogenous catalyst is to anchor the soluble catalyst on to large surface area inorganic supports.[15,16] Many different solid catalysts such as zeolite and metal oxide can heterogenized homogeneous catalysts.[17,18] Nowadays, core–shell superparamagnetic Fe_3O_4 nanoparticles have been used strongly because of their unique properties including the high surface area, low toxicity, separability and biocompatibility.[19–21] Magnetic separation renders the recycling of catalysts from the solution by external magnetic fields much easier than by filtration and centrifugation. Meanwhile, using of core–shell can prevent the occurrence of aggregation of magnetic Fe_3O_4 nanoparticles, and endow the magnetic materials with favorable biocompatibility.

In this work we have reported the immobilization of *N*,*N*-bis(5-chloromethyl-salicylidene)-1,2-phenylenediamine oxoperoxo molybdenum(VI) (CM-salophMoO(O_2)) onto the surface of amino-modified core–shell supermagnetic nanoparticles, Fe_3O_4@APTMS/CM-salophMoO(O_2). The resulting heterogeneous

[a]*Department of Chemistry, Faculty of Basic Science, University of Mohaghegh Ardabili, 179, Ardabil, Iran. E-mail: bezaatpour@uma.ac.ir*

[b]*Department of Chemistry, Payame Noor University (PNU), Tabriz, Iran*

† Electronic supplementary information (ESI) available: Fig. S1: ^{1}H NMR of *N*,*N*-bis(5-chloromethyl-salicylidene)-1,2-phenylenediamine (5-CM-salop), Fig. S2: ^{1}H NMR of 5-CM-salophMo(O_2)O complex Fig. S3: ^{13}C NMR of 5-CM-salophMo(O_2)O complex. See DOI: 10.1039/c5ra27751e

catalysis has been characterized by using different techniques. We have been studying for selective alkene epoxidations, using *tert*-butyl hydroperoxide (70% aqueous) as oxidant. The catalytic performances of supported catalyst have been compared to homogeneous analogues. The reusability of prepared catalysis based on core–shell supermagnetic nanoparticles was also studied in the epoxidation of cyclooctene with *tert*-butyl hydroperoxide in 1,2-DCE.

Experimental section

Materials and physical measurements

All reagent used were purified using known procedures. 5-Chloromethyl-salicylaldehyde[22] have prepared according to literature procedures. 1,2-Phenylenediamine, cyclooctene, cyclohexene, styrene, indene, α-pinene, 1-hepten, 1-octene, 1-dodecen, *trans*-stilben, 3-aminopropyltrimethoxysilane (APTMS), iron(II)chloride ($FeCl_2 \cdot 4H_2O$), iron(III)chloride ($FeCl_3 \cdot 6H_2O$), and ammoniumhydroxide (25% [w/w]) were purchased from Merck Chemical Company. ^{1}H NMR spectra were recorded using a Bruker FT NMR 500 (500 MHz) spectrophotometer $(CD_3)_2SO$. Elemental analyses (carbon, hydrogen and nitrogen) were performed using a Heraeus Elemental Analyzer CHN-O-Rapid (Elementar-Analysesysteme, GmbH). Atomic absorption analysis was carried out on a shimadzu 120 spectrophotometer. The purity of the solvents, cyclooctene, cyclohexene, styrene, indene, α-pinene, 1-hepten, 1-octene, 1-dodecen, *trans*-stilben and analysis of the oxidation products was determined by gas chromatography using Agilent 7890 with a capillary column and FID detector. Column temperature was programmed between 180 °C and 200 °C (2 °C min^{-1}). Nitrogen was used as carrier gas (40 ml min^{-1}) at injection temperature. FT-IR spectra were obtained by Shimadzu 8400S spectrophotometer in KBr pellets. Diffuse reflectance spectra (DRS) were taken on a Scinco 4100 the range 200–1100 nm using $BaSO_4$ as reference. The powder small angle X-ray diffraction studies were done on ITALSTRUCTURE X-ray diffractometer with CuKα (λ = 1.54 Å) radiation. The voltage and current applied to the X-ray tube were 40 kV and 30 mA, respectively, with scanning speed as 0.001° min^{-1}. Surface morphology and distribution of particles were studied *via* VEGA-TESCAN scanning electron microscopy, using an accelerating voltage of 20 kV.

Preparation of Fe_3O_4@APTMS

The chemical co-precipitation was used for preparation of Fe_3O_4 nanoparticles.[23] Then silica coated Fe_3O_4 NPs (Fe_3O_4@SiO_2) synthesized by the hydrolysis of tetraethylorthosilicate (TEOS) using the sol–gel process.[24] A suspension of Fe_3O_4@SiO_2 (0.5 g) was dispersed in ethanol (50 ml), and 3-aminopropyltrimethoxysilane (APTMS) (2.5 ml) dissolved in 50 ml ethanol was added dropwise to the suspension. The reaction mixture was stirred at 70 °C for 5 h. Finally the brown aminated MNPs was separated magnetically and washed with distilled water for several times to remove any unbound APTMS. FT-IR (KBr, cm^{-1}): 3406 [ν(O–H)], 1033 [ν(Si–O–Si)], 575 [ν(Fe–O)].

Preparation of *N*,*N*-bis(5-chloromethyl-salicylidene)-1,2-phenylenediamine (5-CM-saloph) (4)

5-Chloromethyl-2-hydroxybenzaldehyde was prepared and characterized as described in literature.[25] A mixture of salicylaldehyde (0.25 mol), paraformaldehyde (0.15 mol) and 150 ml of conc. HCl was stirred at room temperature for 48 h. The white solid was filtered, washed with 0.5% $NaHCO_3$ solution, dried and recrystallized in petroleum ether. The solution of (2.5 mmol, 0.27 g) 1,2-phenylenediamine in 20 ml dichloromethane was added dropwise to the solution of 5-chloromethyl-salicyaldehyde (5 mmol, 0.85 g) in 20 ml dichloromethane. The mixture was refluxed for 2 h. The orange coloured precipitates were collected, and washed with reaction solvent and then dried in vacuum (yield 1 g, 96%). Anal. calcd for $C_{22}H_{18}N_2O_2Cl_2$: C, 63.61; H, 4.81; N, 6.71. Found: C, 63.81; H, 4.51; N, 6.49. IR (KBr, cm^{-1}): 1654 [ν(C=N)], 3401 [ν(O–H)]. ^{1}H NMR (500 MHz, $CDCl_3$, 25 °C) δ_{ppm}: 11.2 (s, 2H, OH), 8.1 (s, 2H, Ar-CH=N), 6.8–7.5 (m, 10H, Ar), 4.22 (s, 4H, alkane) (ESI, Fig. S1†). ^{13}C NMR (500 MHz,

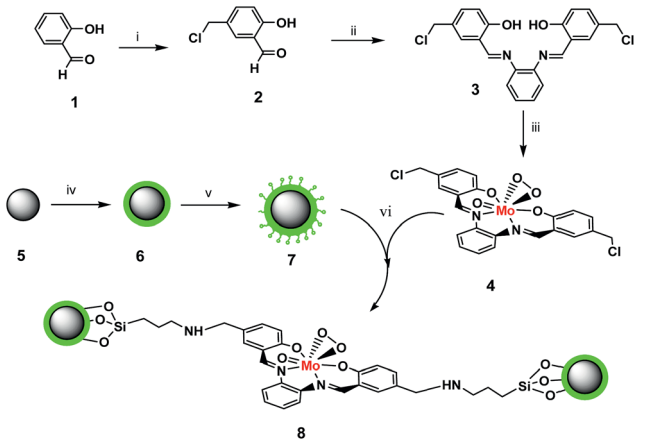

Scheme 1 Preparation of heterogeneous nanocatalyst, (i) paraformaldehyde/HCl (ii) *O*-phenylenediamine (iii) MoO_3/H_2O_2 (iv) $FeCl_2$/$FeCl_3/NH_3$ (v) APTMS (vi) reflux in toluene/24 h.

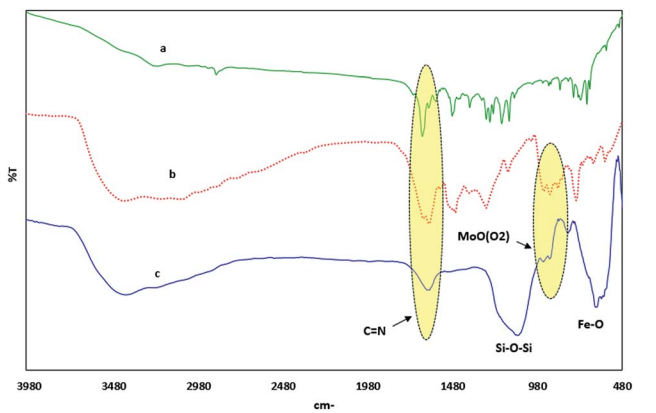

Fig. 1 FT-IR spectrum of (a) 5-CM-saloph Schiff base ligand, (b) $MoO(O_2)$ Schiff base complex, (c) Fe_3O_4@APTMS/CM-salophMoO(O_2).

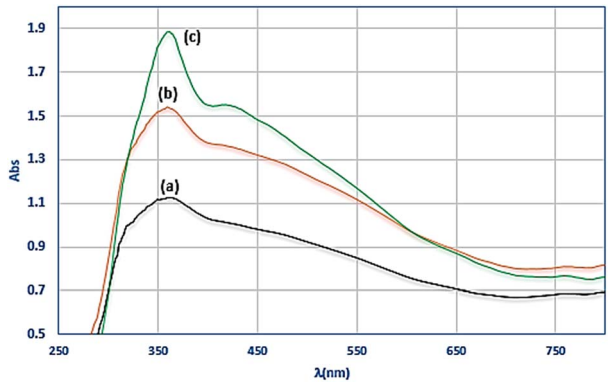

Fig. 2 DRS spectrum of (a) salophMoO(O_2) complex (b) Fe_3O_4@APTMS/CM-salophMoO(O_2), (c) Fe_3O_4@APTMS/CM-salophMoO after catalysis.

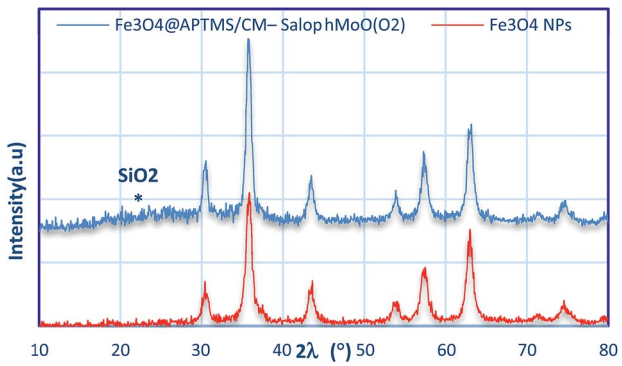

Fig. 3 Small angle X-ray diffraction pattern of: (blue) Fe_3O_4@APTMS/CM-salophMoO(O_2), (red) Fe_3O_4 nanoparticles.

$CDCl_3$): 55.9, 115.2, 118.3, 118.8, 119.6, 120.8, 127.7, 142.5, 152.2, 155.6, 163.3 (ESI, Fig. S2†).

Synthesis of 5-CM-salophen complex of oxoperoxomolybdenum(VI)

The CM-salophMoO(O_2) complex is synthesized by dissolving 0.72 g of MoO_3 (5 mmol) in hydrogen peroxide (30%, 10 ml) by stirring at room temperature. Then the *N*,*N*-bis(5-chloromethyl-salicylidene)-1,2-phenylenediamine (5 mmol) dissolved in a minimum volume of methanol and added the above solution under stirring gave yellow solid. The solid was filtered off, washed with water, methanol and finally with diethyl ether and dried *in vacuo* (yield 55%). Anal. calcd for $C_{22}H_{16}N_2O_5Cl_2Mo$: C, 47.42; H, 3.26; N, 5.03; Mo, 17.23. Found: C, 47.01; H, 3.50; N, 4.7; Mo, 16.95. IR (KBr, cm^{-1}): 1620 [ν(C=N)], 860 [ν(O–O)] and 944 [ν(Mo=O)]. ^{1}H NMR (500 MHz, DMSO-d_6, 25 °C) δ_{ppm}: 8.6, 8.7 (s, 2H, Ar-CH=N), 6.8–7.8 (m, 10H, Ar), 4.3, 4.4 (s, 4H, alkane) (ESI, Fig. S3†). ^{13}C NMR (500 MHz, DMSO-d_6): 56.1, 57.1, 111.2, 111.7, 112.8, 114.6, 116.1, 117.5, 118.6, 119.6, 121.4, 123.2, 124.6, 143.2, 144.3, 155.4, 156.4, 161.2, 162.7, 166.3, 167.2, 169.3 (ESI, Fig. S4†). DRS (solid phase, nm): 368 and 435 nm.

Preparation of Fe_3O_4@APTMS/CM-salophMoO(O_2)

A solution containing the CM-salophMoO(O_2) complex (5 mmol, in 50 ml toluene) was added to a suspension of amine-functionalized Fe_3O_4@APTMS (1.0 g in 50 ml toluene). The resulting mixture was stirred at 70 °C for 24 h. After cooling, the brown Fe_3O_4@APTMS/CM-salophMoO(O_2) nanocatalyst was separated using an external magnet and washed several times with water and ethanol.

Epoxidation of alkenes by catalyst

Epoxidation of alkenes such as cyclooctene, cyclohexene, styrene, indene, α-pinene, 1-hepten, 1-octene, 1-dodecen, *trans*-stilben using homogeneous and heterogeneous form of catalyst was carried out in a 25 ml Schlenk tube. All glassware's were oven-dried prior to use. The system was purged with argon gas. In a typical experiment, a mixture of 0.2 g of Fe_3O_4@APTMS/CM-salophMo(O_2)O (2.3×10^{-5} mol for net complex), and 1, 2-dichloroethane (DCE) (5 ml), 5 mmol freshly distilled alkenes and 12.5 mmol of TBHP was refluxed for 2 h. The reaction followed by separation of the catalyst using an external magnetic field (for heterogeneous catalyst). The separated catalyst washed with absolute ethanol could be reused after drying at 80 °C under vacuum. 1,2-Dichlorobenzene was used as an internal standard. The solution was then injected to GC analysis.

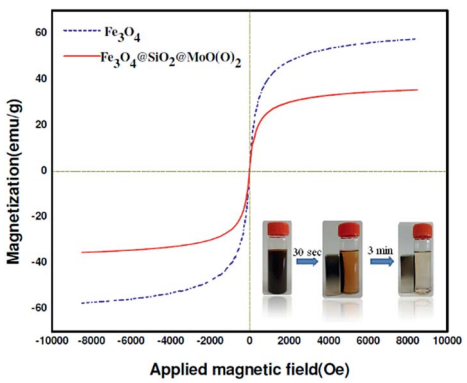

Fig. 4 Magnetization curves at 298 K for Fe_3O_4 (dot) and Fe_3O_4@APTMS/CM-salophMoO(O_2) (solid).

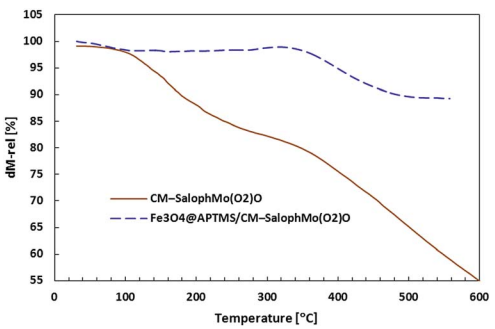

Fig. 5 TG curve of Fe_3O_4@APTMS/CM-salophMoO(O_2) (dash) and CM-salophMoO(O_2) (solid).

Result and discussion

Synthesis and characterization

Scheme 1 shows the synthesis of tetradentate Schiff base (derived from 5-chloromethylsalicyaldehyde and 1,2-phenylenediamine) oxo–peroxomolybdenum(VI) complex and immobilization of complex on Fe_3O_4/SiO_2 core–shell nanoparticles as a heterogeneous recyclable nanocatalyst.

^{1}H NMR of Schiff base ligand and Mo complex confirm the formation of compounds **3** and **4**. In the ^{1}H NMR spectra of the Schiff base ligand the signal at 11.2, 8.1 and 4.22 assigned for H-phenol, H-imine and H-methylene respectively. By considering of the ^{1}H NMR and ^{13}C NMR spectra of Mo(VI) complex it seems that the more splitting is shown because of the non-equivalence chelate ring.

There is some additional information from a comparison of the infrared spectra of the Schiff base ligand, corresponding $MoO(O_2)$ complex and Fe_3O_4@APTMS/CM-salophMoO$_2$ (Fig. 1).

The FT-IR spectrum of CM-saloph Schiff base ligand exhibit the C=N stretching vibration intense band at 1654 cm$^-$, which shift to 1632 and 1630 cm^{-1} in the corresponding CM-salophMoO(O_2) complex and Fe_3O_4@APTMS/CM-salophMoO(O_2) respectively, indicating coordination of azomethine nitrogen.[26] Also the ν(Mo=O) and ν(O–O) vibrations of CM-salophMoO(O_2) complex appear around 929 cm^{-1} and 860 cm^{-1} respectively.[27] The appearance of two bands in Fig. 1(c) at 1100 and 592 cm^{-1} can be assigned to Si–O–Si and Fe–O stretching, respectively. Comparison of all the FT-IR data suggest that the $MoO(O_2)$ group is bonded to the Schiff base ligand and then supported successfully on Fe_3O_4@APTMS.

The diffuse reflectance spectra (DRS) of the $MoO(O_2)$ complex and Fe_3O_4@APTMS/CM-salophMoO(O_2) in Fig. 2 show two bands at 368 and 435 nm to assigned n–π^* of Schiff base ligand and ligand-to metal charge transfer transitions, respectively.[14,28] So the comparison of diffuse reflectance spectra (DRS) of the Fe_3O_4@APTMS/CM-salophMoO(O_2) and CM-salophMoO(O_2) show that there is not any geometrical change in oxo–peroxomolybdenum(VI) complex after supporting on Fe_3O_4@APTMS NPs.

The atomic absorption analysis gives the Mo content of heterogeneous catalyst 3.5 wt%.

As shown in Fig. 3, the X-ray diffraction pattern of crystalline structures of Fe_3O_4 NPs and core–shell magnetic Fe_3O_4@APTMS/CM-salophMoO(O_2) show characteristic diffraction peaks correspond to (220), (311), (400), (422), (511) and (440) reflections of inverse spinel Fe_3O_4 NPs, respectively. It showed characteristic peaks, and the relative intensity matched well with those of standard Fe_3O_4 nanoparticles (reference JCPDS card no. 87-2334). The week broad peak appeared in the range from $2\theta =$ 19 to 27 indicates the existence of amorphous silica. The crystal size of Fe_3O_4 NPs and core–shell magnetic Fe_3O_4@APTMS/CM-salophMoO(O_2) were determined by using the Debye–Scherrer ($d_{\{hkl\}} = 0.94\lambda/\beta \cos\theta$) equation where β is the half-width of the highest intensity X-ray diffraction lines, d is the average crystalline diameter, 0.94 is the Scherrer constant, θ is the Bragg angle in degree and λ is the X-ray wavelength. Here, the (311) peak of the highest intensity was selected and d_{311} obtained 25 nm for Fe_3O_4 NPs. Comparing between X-ray diffraction pattern of Fe_3O_4 NPs and Fe_3O_4@APTMS/CM-salophMoO(O_2) shows that the coating of silica and salophMoO(O_2) complex on Fe_3O_4 NPs did not significantly affect the structure of NPs.

As shown in Fig. 4, the plots of magnetization *versus* magnetic field show the absence of hysteresis phenomenon and indicate that product has superparamagnetism at room temperature. Fe_3O_4 and Fe_3O_4@APTMS/CM-salophMoO(O_2) show the magnetic saturation is 55.6 and 38.12 emu g^{-1}, respectively. These results indicated that the magnetization of Fe_3O_4 decreased considerably with the increase of SiO_2 and

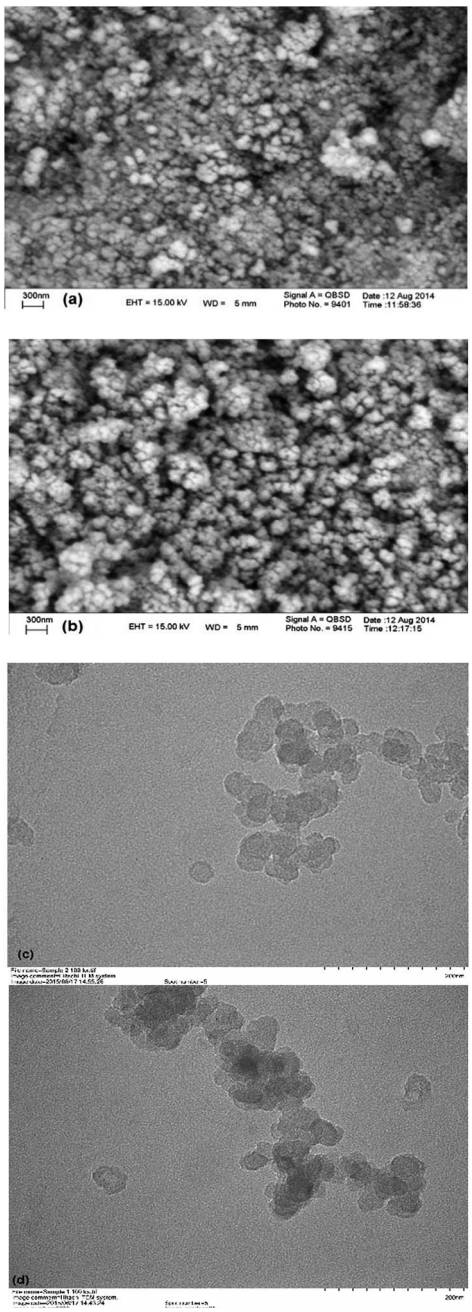

Fig. 6 SEM images of (a) Fe_3O_4 NPs, (b) Fe_3O_4@APTMS/CM-salophMoO(O_2) and TEM images of (c) Fe_3O_4 NPs, (d) Fe_3O_4@APTMS/CM-salophMoO(O_2).

Table 1 Optimization of Fe_3O_4@APTMS/CM-salophMoO(O_2) catalytic condition, solvent = 5 ml; duration = 30 min with the molar ratio of cyclooctene : oxidant are 1 : 2

Solvent	Amount of catalyst (g)	T (°C)	Oxidant	Conversion (%)/ selectivity (%)
1,2-DCE	Without cat.	80	TBHP	26/100
1,2-DCE	0.005	80	TBHP	56/100
1,2-DCE	0.01	80	TBHP	75/100
1,2-DCE	0.02	80	TBHP	97/100
1,2-DCE	0.025	80	TBHP	97/100
1,2-DCE	0.02	70	TBHP	87/100
1,2-DCE	0.02	60	TBHP	77/100
1,2-DCE	0.02	40	TBHP	60/100
CH_3CN	0.02	80	TBHP	82/100
CH_3OH	0.02	Reflux	TBHP	60/100
CH_2Cl_2	0.02	Reflux	TBHP	58/100
1,2-DCE	0.02	80	UHP	55/100
1,2-DCE	0.02	80	$NaIO_4$	34/100

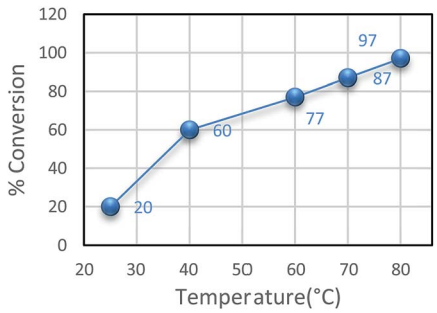

Fig. 7 The effect of reaction temperature on conversion of cyclooctene.

$Mo(O)_2$ Schiff base complex. However, the Fe_3O_4@APTMS/CM-salophMoO$_2$ can still be separated from the solution by using an external magnetic field.

Thermogravimetric analysis have been used to understanding of thermal stability of supported catalyst. As shown in Fig. 5, the decomposition of the CM-salophMoO(O_2) complex and Fe_3O_4@APTMS/CM-salophMoO(O_2) catalyst were began 150 °C and 360 °C respectively. These criteria indicate that the Fe_3O_4@APTMS/CM-salophMoO(O_2) catalyst is thermally stable than CM-salophMoO(O_2).

Fig. 6 illustrates the SEM (Fig. 6(a and b)) and TEM (Fig. 6(c and d)) images of Fe_3O_4 and Fe_3O_4@APTMS/CM-salophMoO$_2$. The size and morphology of the nanoparticles were observed using transmission electron microscopy (TEM). TEM images show that the particle size has changed after immobilization of complex on modified MNPs. The synthesized catalysts are well dispersed and most of the nanoparticles are almost spherical in shape. The average particle size estimated about 29 nm and 41 nm for Fe_3O_4 and Fe_3O_4@APTMS/CM-salophMoO$_2$ respectively.

Epoxidation catalytic reactivity of CM-salophMoO(O_2) (4) and Fe_3O_4@APTMS/CM-salophMoO(O_2) (8)

Catalytic reactivity of heterogeneous, Fe_3O_4@APTMS/CM-salophMoO(O_2) and homogeneous, CM-salophMoO(O_2) catalysts were tested for the selective epoxidation of cyclooctene, cyclohexene, styrene, indene, α-pinene, 1-hepten, 1-octene, 1-dodecen and *trans*-stilben using *tert*-butylhydroperoxide (70% aqueous) as oxidant. The catalytic activities of Fe_3O_4@APTMS/CM-salophMoO(O_2) were optimized for epoxidation of cyclooctene through investigation of the influence of solvent, the reaction temperature, the molar ratio of [TBHP]/[cyclooctene] and the time of epoxidation reaction. For selecting the best solvent, dichloromethane, methanol, acetonitrile, dichloroethane were employed as solvents. The optimizing results in Table 1 show that dichloroethane to be the best solvent. Apparently, highly coordinating solvents, such as CH_3OH, cause a significant decrease in the catalytic activity since they compete with TBHP for binding to the Mo center.[29] It seems that the lower reflux reaction temperature is the important reason of lowest conversion in CH_2Cl_2 (60%). The conversion increased with increasing the reaction temperature from 25 °C to 80 °C (Fig. 7).

Fig. 8 shows that the nanoparticles have good separation and dispersion by ultrasonication. After of ultrasonication the catalytic reactivity was tested and conversion increases during ultrasonication time form 32–100%.

The percent of conversion increased with increasing the molar ratio of [TBHP] : [cyclooctene] from 0.5 to 2 and the conversion of cyclooctene was maximum at 2 : 1 molar ratio of [TBHP] : [cyclooctene] (Fig. 9).

In this research work, different oxidants such as $NaIO_4$, UHP (urea–H_2O_2) and TBHP (*tert*-butylhydroperoxide) were examined in epoxidation of cyclooctene in variable solvents. TBHP has some advantageous: (i) it can give high percent of conversion; (ii) environment-friendly; (iii) it has good thermal stability. Table 1 shows that TBHP as the oxygen donor has the highest conversion in the optimized reaction condition. Hence, typical catalytic reaction conditions involve 1,2-DCE (5 ml) solutions at 80 ±

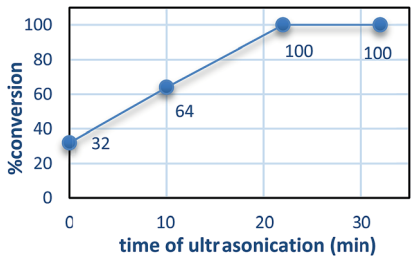

Fig. 8 Effect of catalyst dispersion by ultrasonication before catalytic process.

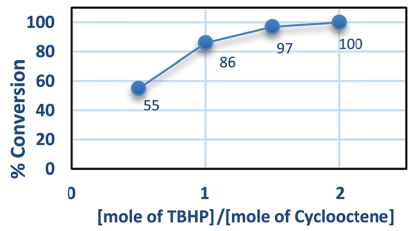

Fig. 9 Effect of [TBHP]/[cyclooctene] ratio on cyclooctene conversion at 80 °C.

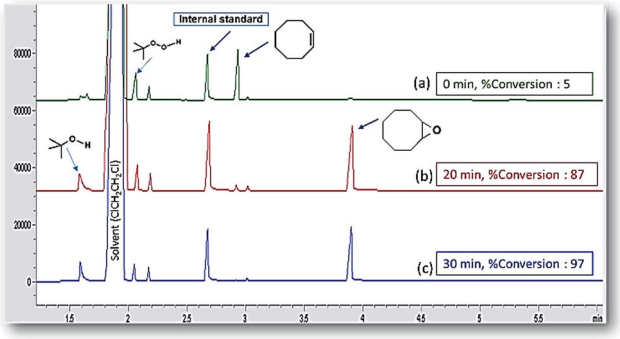

Fig. 10 Typical chromatogram taken during of catalytic process, reaction time (a) 0 min, (b) 20 min and (c) 30 min with 100% selectivity.

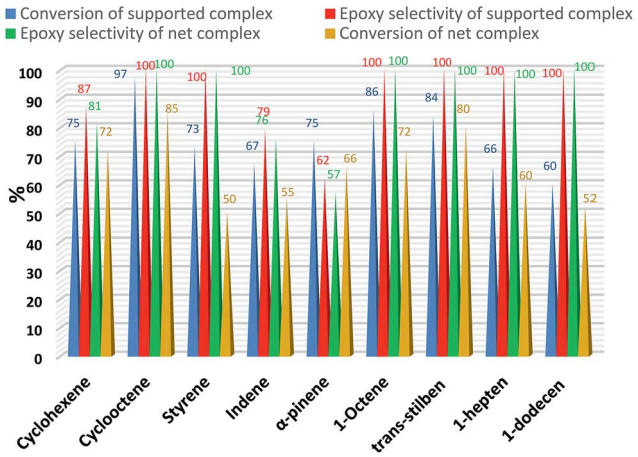

Fig. 11 Product distributions in the epoxidation of various alkenes using net complex and heterogeneous complex.

2 °C, alkene (5 mmol), TBHP (12.5 mmol) with the molar ratio of cyclooctene : TBHP and catalyst (0.0074 mmol), 0.02 g for Fe_3O_4@APTMS/CM-salophMoO(O_2) stirred for 30 min for cyclooctene and 60 min for the other olefins. The final solution exhibited no color. So, no presence of metal was detected in the solution after using heterogeneous catalyst, (it was confirmed by atomic absorption spectroscopy). The product distributions in the epoxidation of various alkenes using net complex and heterogeneous catalysts are shown in Fig. 11. Generally, one of the main problems of homogeneous transition metal complexes as catalysts is the formation of oxo and peroxo dimeric and other polymeric species. The formation of these compounds can deactivate catalysts irreversibly. As shown in Fig. 11, Fe_3O_4@APTMS/CM-salophMoO(O_2) gives higher percent of conversion of alkenes than the CM-salophMoO(O_2) complex.

Fig. 10 shows the chromatograms of the cyclooctene oxidation proceeds with a moderate 100% selectivity for epoxidation with 97% conversion in 30 min for Fe_3O_4@APTMS/CM-salophMoO(O_2) catalyst. In the event that the CM-salophMoO(O_2) complex shows 75% conversion in the same condition. This trend was illustrated for all alkenes in Fig. 11. Catalytic reactions were not affected by the presence or absence of light. The catalytic oxidation of substrate with TBHP in the absence of catalysts (blank run) occurs with low conversion (~26%). We were able to separate supermagnetically nanocatalyst by using external magnetic field and use the catalyst at least five successive times without significant decrease in conversion (Table 2).

Scheme 2 shows a proposed mechanism *via* an interaction between the olefin HOMO $\pi_{(C=C)}$ and the unoccupied $\sigma^*_{(O-O)}$ orbital of peroxo complex.[40,41] In the first step, the electron density is redistributed from the C–C bonding olefin orbital to $\sigma^*_{(O-O)}$ orbital *via* breaking of O–O bond and then epoxide is generated. After that, proton of TBHP is transferred to the terminal of oxo atom of the MoO_2 and *t*-BuOO$^-$ is coordinated to Mo(VI) as a Lewis acidic metal center. Finally, forming of hydrogen bond between the coordinated *t*-BuOO$^-$ and OH, releases catalyst and alcohol. Table 3 compares the efficiency of our catalyst with some found in the literature. The illustrated Fe_3O_4@APTMS/CM-salophMoO(O_2) catalytic system is one of the fastest magnetically recoverable catalytic system for epoxidation of alkenes. Our novel catalyst showed higher catalytic activity than the $[MoO(O_2)_2(H_2O)$ (ONnDodec$_3$)],[30] $[MoO(O_2)_2$(HMPT)],[31] $[Mo(O)(O_2)_2$(bipy)][32] and $[MoO_2(py)_2]$-MCM41(ref. 34) for the epoxidation of cyclooctene. So the comparison of epoxidation reaction time of our catalyst (30

Table 2 The results obtained from catalyst reuse in the epoxidation of cyclooctene[a]

Run	% conversion[a]	% epoxy[a]	% Mo leached[b]
1	100	100	0
2	100	100	0
3	99	100	0
4	99	100	0
5	99	100	0

[a] Catalytic condition, solvent = 5 ml; duration = 30 min with the molar ratio of cyclooctene : oxidant are 1 : 2. [b] Detected by atomic absorption spectroscopy.

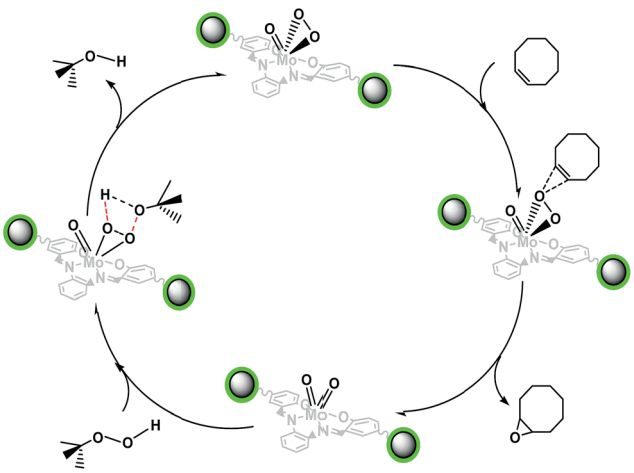

Scheme 2 Proposed mechanism for alkene epoxidation by the Fe_3O_4@APTMS/CM-salophMo(O_2)O.

Table 3 Comparison of literature reports on the epoxidation of cyclooctene under various conditions

Catalyst	Reaction conditions	% epoxy	Ref.
$[MoO(O_2)_2(H_2O)(ONnDodec_3)]$	H_2O_2/CH_3CN/24 h	75	30
$[MoO(O_2)_2(HMPT)]$	H_2O_2/DCE/5 h	14	31
$[Mo(O)(O_2)_2(bipy)]$	UHP/C_4mim(PF_6)/8 h	90	32
$[Mo(O)(O_2)_2(dmpz)_2]$	H_2O_2/CH_3Cl/18 h	86	33
$[MoO_2(py)_2]$-MCM41	TBHP/$CHCl_3$/7 h	89	34
MoO_2acpyAmpMCM-41	TBHP/$CHCl_3$/4h	99	35
$[Mo(O)(O_2)_2$(L-L)]SMNPs	TBHP/CH_3Cl/6 h	96	36
MoO_2-thio-SCMNPs	TBHP/$CHCl_3$/24 h	100	37
Mag-Mo-nanocatalyst	TBHP/CCl_4/5 h	99	38
MoO_2(L)(EtOH)ZBS-PVPA	TBHP/DCE/8h	100	39
Fe_3O_4@APTMS/ CM-salophMoO(O_2)	TBHP/DCE/30 min	97	This work

min) with the other reports (4 h),[35] (24 h),[37] (5 h)[38] and (8 h)[39] is many considerable.

Conclusions

As a part of our progressing studies on the catalyst, Novel ancillary branch coated of oxo–peroxo Mo(VI) tetradentate Schiff base complex on superparamagnetic nanoparticles was prepared successfully and characterized by physico-chemical methods. The solids containing immobilized Mo(VI) tetradentate Schiff base complex has been studied as efficient heterogeneous nanocatalyst for chemoselective epoxidation of olefins. Oxidation result of Fe_3O_4@APTMS/CM-salophMoO(O_2) was comparable with net CM-salophMoO(O_2). In this report the conversion of heterogeneous catalyst was greater then the homogenous catalyst for all of olefins epoxidation. Also the Fe_3O_4@APTMS/CM-salophMoO(O_2) can be separated by using a small external magnetic field from the reaction system and reused for at least 5 times without significant decrease in conversion. Our novel catalyst showed higher catalytic activity than the other Mo(VI) complexes reported in literature.[30–39] The illustrated superparamagnetic catalyst shows excellent conversion (97%) in 30 min.

Acknowledgements

Authors are grateful to the Research Council of Mohaghegh-e-Ardabili University for their financial support.

Notes and references

1 (*a*) K. A. Srinivas, A. Kumar and S. M. S. Chauhan, *Chem. Commun.*, 2002, 2456–2457; (*b*) M. R. dos Santos, J. R. Diniz, A. M. Arouca, A. F. Gomes, F. C. Gozzo, S. M. Tamborim, A. L. Parize, P. A. Z. Suarez and B. A. D. Neto, *ChemSusChem*, 2012, **5**, 716–726; (*c*) D. M. Boghaei, A. Bezaatpour and M. Behzad, *J. Mol. Catal. A: Chem.*, 2006, **245**, 12–16; (*d*) J. Rahchamani, M. Behzad, A. Bezaatpour, V. Jahed, G. Dutkiewicz, M. Kubicki and M. Salehi, *Polyhedron*, 2011, **30**, 2611–2618.

2 (*a*) A. Lazar, W. R. Thiel and A. P. Singh, *RSC Adv.*, 2014, **4**, 14063–14073; (*b*) G. Fioroni, F. Fringuelli, F. Pizzo and L. Vaccaro, *Green Chem.*, 2003, **5**, 425–428; (*c*) M. C.-Y. Tang, K.-Y. Wong and T. H. Chan, *Chem. Commun.*, 2005, **50**, 1345–1347.

3 J. A. Brito, M. Go'mez, G. Muller, H. Teruel, J. Clinet, E. Duñach and M. A. Maestro, *Eur. J. Inorg. Chem.*, 2004, 4278–4285.

4 A. V. Biradar, M. K. Dongare and S. B. Umbarkar, *Tetrahedron Lett.*, 2009, **50**, 2885–2888.

5 R. J. Cross, P. D. Newman, R. D. Peacock and D. Stirling, *J. Mol. Catal. A: Chem.*, 1999, **144**, 273–284.

6 V. Conte, F. Di Furia and G. Modena, in *Organic Peroxides*, ed. W. Ando, Wiley, Chichester, 1992, pp. 559–598.

7 R. Curci and J. O. Edwards, in *Catalytic Oxidations with Hydrogen Peroxide as Oxidant*, ed. G. Strukul, Kluwer, Dordrecht, 1992, pp. 57–60.

8 J. A. L. da Silva, J. J. R. F. da Silva and A. J. L. Pombeiro, *Coord. Chem. Rev.*, 2011, **255**, 2232–2248.

9 (*a*) K. A. Jorgensen, *Chem. Rev.*, 1989, **89**, 431–458; (*b*) J. M. Brégeault, *J. Chem. Soc., Dalton Trans.*, 2003, 3289–3302.

10 (*a*) K. J. Balkus Jr, A. K. Khanrnamedova, K. M. Dixon and F. Bedioui, *Appl. Catal., A*, 1996, **143**, 159–173; (*b*) R. Belal and B. Meunier, *J. Mol. Catal.*, 1988, **44**, 187–190; (*c*) M. Salavati-Niasari, M. Shakouri-Arani and F. Davar, *Microporous Mesoporous Mater.*, 2008, **116**, 77–85; (*d*) K. O. Xaviera, J. Chackoa and K. K. Mohammed Yusuff, *Appl. Catal., A*, 1996, **258**, 251–259.

11 K. J. Ballus Jr, A. K. Khanmamedova, K. M. Dixon and F. Bedioui, *Appl. Catal., A*, 1996, **143**, 159–173.

12 (*a*) A. Bezaatpour, M. Amiri and V. Jahed, *J. Coord. Chem.*, 2011, **64**, 1837–1847; (*b*) A. Bezaatpour, *React. Kinet., Mech. Catal.*, 2014, **112**, 453–465.

13 A. Hu, S. Liu and W. Lin, *RSC Adv.*, 2012, **2**, 2576–2580.

14 (*a*) A. Bezaatpour, M. Behzad, V. Jahed, M. Amiri, Y. Mansoori, Z. Rajabalizadeh and S. Sarvi, *React. Kinet., Mech. Catal.*, 2012, **107**, 367–381; (*b*) M. Bagherzadeh and M. Zare, *Coord. Chem.*, 2013, **66**, 2885–2900.

15 C. Baleizão, B. Gigante, D. Das, M. Álvaro, H. Garcia and A. Corma, *Catalysis*, 2004, **223**, 106–113.

16 C. A. McNamara, M. J. Dixion and M. Bradely, *Chem. Rev.*, 2002, **102**, 3275–3300.

17 H. V. Bekkum and J. C. Vander Waal, *J. Mol. Catal. A: Chem.*, 1997, **124**, 137–146.

18 S. Imamura, H. Sakai, M. Shono and H. Kanai, *Catalysis*, 1998, **177**, 72–81.

19 Y. S. Lin and C. L. Haynes, *Chem. Mater.*, 2009, **21**, 3979–3986.

20 M. Mahmoudi, S. Sant, B. Wang, S. Laurent and T. Sen, *Adv. Drug Delivery Rev.*, 2011, **63**, 24–46.

21 M. Sevilla, T. Valdés-Solis, P. Tartaj and A. B. Fuertes, *J. Colloid Interface Sci.*, 2009, **340**, 230–236.

22 T. Joseph, D. Srinivas, C. S. Gopinath and S. B. Halligudi, *Catal. Lett.*, 2002, **83**, 209–214.

23 Z. G. Peng, K. Hidajat and M. S. Uddin, *J. Colloid Interface Sci.*, 2004, **271**, 277–283.
24 L. Chen, B. Li and D. Liu, *Catal. Lett.*, 2014, **144**, 1053–1061.
25 A. Z. El-Sonbati, A. A. El-Bindary and I. G. Rashed, *Spectrochim. Acta, Part A*, 2002, **58**, 1411–1424.
26 W. E. Hill, N. Atabay, C. A. McAuliffe, F. P. McCullough and S. M. Razzoki, *Inorg. Chim. Acta*, 1979, **35**, 35–41.
27 N. Gharah, S. Chakraborty, A. K. Mukherjee and R. Bhattacharyya, *Inorg. Chim. Acta*, 2009, **362**, 1089–1100.
28 M. Bagherzadeh, M. Zare, V. Amani, A. Ellern and L. K. Woo, *Polyhedron*, 2013, **53**, 223–229.
29 F. E. Kühn, M. Groarke, E. Bencze, E. Herdtweck, A. Prazeres, A. M. Santos, M. J. Calhorda, C. C. Romão, I. S. Gonçalves, A. D. Lopes and M. Pillinger, *Chem.–Eur. J.*, 2002, **8**, 2370–2383.
30 G. Wahl, D. Kleinhenz, A. Schorm, J. Sundermeyer, R. Stowasser, C. Rummey, G. Bringmann, C. Fickert and W. Kiefer, *Chem.–Eur. J.*, 1999, **5**, 32–37.
31 M. Quenard, V. Bonmarin and G. Gelbard, *Tetrahedron Lett.*, 1987, **28**, 2237–2238.
32 M. Herbert, F. Montilla, R. Moyano, A. Pastor, E. Álvarez and A. Galindo, *Polyhedron*, 2009, **28**, 3929–3934.
33 M. Herbert, F. Montilla and A. Galindo, *J. Mol. Catal. A: Chem.*, 2011, **338**, 111–120.
34 A. Sakthivel, Y. Sakthivel, F. M. Pedro, A. S. T. Chiang and F. E. Kuhn, *Appl. Catal., A*, 2005, **281**, 267–273.
35 M. Masteri-Farahani, F. Farzaneh and M. Ghandi, *J. Mol. Catal. A: Chem.*, 2006, **248**, 53–60.
36 S. Shylesh, J. Schweizer, S. Demeshko, V. Schünemann, S. Ernst and W. R. Thiel, *Adv. Synth. Catal.*, 2009, **351**, 1789–1795.
37 M. Mohammadikish and M. Masteri-Farahani, *J. Magn. Magn. Mater.*, 2014, **354**, 317–323.
38 Y. Shokouhimehr, J. Piao, Y. Kim and M. Jang, *Angew. Chem.*, 2007, **119**, 7169–7176.
39 Y. Li, X. Fu, B. Gong, X. Zou, X. Tu and J. Chen, *J. Mol. Catal. A: Chem.*, 2010, **322**, 55–62.
40 I. V. Yudanov, C. D. Valentin, P. Gisdakis and N. Rosch, *J. Mol. Catal. A: Chem.*, 2000, **158**, 189–197.
41 M. Bagherzadeh, M. Amini, H. Parastar, M. Jalali-Heravi, A. Ellern and L. K. Woo, *Inorg. Chem. Commun.*, 2012, **20**, 86–89.